Shock Fitting Method for Complicated Two-Dimensional Supersonic Flows

Manuel D. Salas*
NASA Langley Research Center, Hampton, Va.

The floating shock fitting technique is examined. Second-order difference formulas are developed for the computation of discontinuities. A procedure is developed to compute mesh points that are crossed by discontinuities. The technique is applied to the calculation of internal two-dimensional flows with arbitrary number of shock waves and contact surfaces. A new procedure, based on the coalescence of characteristics, is developed to detect the formation of shock waves. Results are presented to validate and demonstrate the versatility of the technique.

I. Introduction

INVISCID supersonic flows are governed by a first-order quasi-linear hyperbolic system of equations. The numerical computation of these flows is complicated, because the regular solution may break down due to the nonlinearity of the governing equations. The breakdown is characterized by the appearance of surfaces, such as shock waves and vortex sheets, across which the dependent variables or their derivatives are discontinuous. During the last decade, 2 numerical techniques have emerged for the analysis of these flows. One, known as shock capturing, tries to remove the explicit computation of the discontinuties by generalizing the concept of a solution of the Euler equations to include weak solutions (i.e., discontinuities). Because the shock capturing scheme requires no special treatment to deal with discontinuties, it has become an extremely popular way of computing. However, despite its present popularity, the results obtained with this technique[1] force us to agree with Moretti's conclusion that shock capturing is a poor interpretation of a physical phenomenon, and an extremely uneconomical way of computing.[3]

The other technique, known as shock fitting, makes special provisions for explicitly computing the discontinuties. In essence, it locates the discontinuties and treats them as boundaries between regions where a regular solution is valid. The effectiveness and soundness of this approach has been proven for a large number of problems involving 2, 3, and 4 independent variables. However, for problems in 3 or more independent variables, the partitioning of a flowfield into regions where a regular solution is valid, can create some difficult topological problems.[3] Recently, Moretti[4] has developed a technique (reminiscent of that proposed by Richtmyer and Morton,[5] that treats the discontinuities explicitly but does not require them as boundaries of the flow. This therefore eliminates the problems associated with partitioning the flowfield. It is this technique, known as floating shock fitting, that forms the subject matter of this paper.

To avoid unnecessary complications, the technique will be discussed in the context of a two-dimensional problem. However, to demonstrate the capabilities of the technique, results from complex flowfields are presented.

Presented as Paper at the AIAA 2nd Computational Fluid Dynamics Conference, submitted June 20, 1975; revision received September 17, 1975.

Index categories: Nozzle and Channel Flow; Shock Waves and Denotations; Supersonic and Hypersonic Flow.

*Aero-Space Technologist, Aerodynamic Analysis Section, Hypersonic Aerodynamics Branch, High-Speed Aerodynamics Division. Member AIAA.

II. Problem Definition

We will discuss the floating shock fitting technique as it applies to the flow of an inviscid, perfect gas through a two-dimensional duct of arbitrary geometry. The flow is assumed to be supersonic throughout, and consequently, irregular shock reflections are not considered. Shock waves generated by either discontinuties in the slopes of the walls, or by coalescence of pressure waves, will be automatically detected and fitted into the calculation. The number of shock waves, contact surfaces, and the number of interactions of these discontinuties, is considered arbitrary (limited only by computer storage).

III. Governing Equations

The flow variables are nondimensionalized by scaling the pressure, density, and temperature, with respect to their initial values (p_i, ρ_i, T_i), scaling the velocities with respect to $(p_i/\rho_i)^{1/2}$, and scaling all lengths with respect to some arbitrary reference length. The Euler equations written in a Cartesian frame (r,z), with the z-axis running along the length of the duct, are

$$P_z + (uwP_r + \gamma w u_r - \gamma u w_r)/\beta = 0$$

$$w_z + (uww_r - \gamma T u_r - TuP_r)/\beta = 0$$

$$u_z + (uu_r + TP_r)/w = 0$$

$$S_z + uS_r/w = 0 \tag{1}$$

Where P is the natural logarithm of pressure, u and w are the velocity components in the r and z directions, respectively; S is the entropy, γ is the ratio of specific heats; the temperature is given by

$$T = \exp((S + (\gamma - 1)P)/\gamma) \tag{2}$$

and $\beta = w^2 - \gamma T$.

The following equations are introduced here for later reference. By combining the 2 momentum equations, we get

$$\tau_z + \frac{w^2 \tau \tau_r}{\beta} + \left(1 + \frac{\tau^2 w^2}{\beta}\right)\frac{TP_r}{w^2} = 0 \tag{3a}$$

where $\tau = u/w$. With Eq. (3a) and the continuity equation in the form

$$P_z + w^2(\tau P_r + \gamma \tau_r)/\beta = 0 \tag{3b}$$

we can obtain the compatibility equation

$$\tau' \pm ([\gamma T(\beta+w^2\tau^2)]^{1/2}/\gamma w^2)P' = 0 \tag{4}$$

where the primes denote differentiation along the characteristic directions

$$\lambda^{\pm} = (w^2\tau \pm [\gamma T(\beta+w^2\tau^2)]^{1/2})/\beta \tag{5}$$

The Euler Eqs. (1) are recast in terms of computational coordinates (X,Z) defined by

$$X=(r-b(z))/(c(z)-b(z)) \quad Z=z \tag{6}$$

where $r=b(z)$ and $r=c(z)$ define the lower and upper walls of the duct. In matrix form the equations of motion become

$$f_Z = \underline{A} f_X \tag{7}$$

where the vector f is

$$f=\begin{bmatrix} P \\ u \\ w \\ S \end{bmatrix} \tag{8}$$

and the matrix $\underline{A}$ is

$$\underline{A}=\begin{bmatrix} a_{11} & a_{12} & a_{13} & 0 \\ a_{21} & a_{22} & 0 & 0 \\ a_{31} & a_{32} & a_{11} & 0 \\ 0 & 0 & 0 & a_{22} \end{bmatrix} \tag{9}$$

$$a_{11} = -(uwX_r+\beta X_z)/\beta$$

$$a_{12} = -\gamma w X_r/\beta$$

$$a_{13} = \gamma u X_r/\beta$$

$$a_{21} = -TX_r/w$$

$$a_{22} = -(uX_r+wX_z)/w$$

$$a_{31} = uTX_r/\beta$$

$$a_{32} = \gamma TX_r/\beta$$

IV. Interior Point Computation

Unlike shock fitting, floating shock fitting does not subdivide the computational plane into regions bounded by discontinuities; instead, a single region is used, as illustrated in Fig. 1. In this single region, mesh points are equally spaced, and all discontinuities are allowed to move freely or float over the fixed grid. Their motion is subject only to the governing equations.

Except for the mesh points at the walls and in the neighborhood of a discontinuity, all mesh points are computed using the MacCormack scheme[6] to integrate Eq. (7). For example, consider the section of a duct, in the computational plane, sketched in Fig. 1. Using the MacCormack scheme, and assuming the solution is known at the Kth steps, $f_{N,K+1}$ is obtained from

level 1

$$\bar{f}_{N,K+1} = f_{N,K} + \underline{A}_{N,K}(f_{N+1,K}-f_{N,K})\Delta Z/\Delta X$$

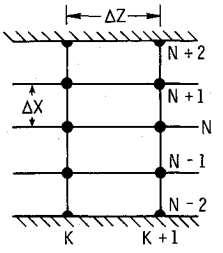

Fig. 1 Computational plane.

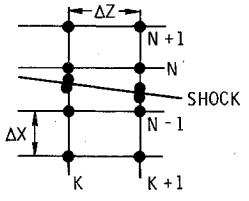

Fig. 2 Computation in the neighborhood of a shock wave.

level 2

$$f_{N,K+1} = \tfrac{1}{2}(f_{N,K}+\bar{f}_{N,K+1}+\underline{\tilde{A}}_{N,K+1}(\bar{f}_{N,K+1}-\bar{f}_{N-1,K+1})\Delta Z/\Delta X) \tag{10}$$

Because the discontinuties are allowed to float over the fixed grid, special provisions must be taken when evaluating the X derivatives of f, at mesh points in the neighborhood of a discontinuity. Consider again the computation of point $(N,K+1)$, but now in the presence of a shock as shown in Fig. 2. There is no difficulty in computing the first level of the MacCormack scheme, since the forward difference

$$f_X = (f_{N+1,K}-f_{N,K})/\Delta X$$

is valid. However, for the second level, the backward difference

$$\tilde{f}_X = (\bar{f}_{N,K+1}-\bar{f}_{N-1,K+1})/\Delta X$$

is not allowed because $\bar{f}$ is not differentiable across the shock. On the other hand, the very simple approximation,

$$\tilde{f}_X = (\bar{f}_{N,K+1}-\bar{f}_{s,K+1})/(X_N-\bar{X}_{s,K+1})$$

where s denotes conditions at the shock, can result in large truncation errors, and the computation becomes unstable. Moretti recommends using an approximation that involves the values at the shock and the 3 neighboring mesh points [Eq. (61) in Ref. 2]. We have not used this approximation, because it makes the numerical domain of dependence point $(N,K+1)$ much larger than it physically is. Instead, we use the following approximation

$$\tilde{f}_X = -[(0.5\epsilon-1)\bar{f}_{N+1,K+1}+0.5\bar{f}_{s,K+1}+0.5(1-\epsilon)\bar{f}_{N,K+1}]/\Delta X \tag{11}$$

where

$$\epsilon = (X_{N,K+1}-\bar{X}_{s,K+1})/\Delta X$$

The truncation error for Eq. (11), (based on f_X, not f) is given by

$$(\epsilon+2)(\epsilon-1)\Delta X/4 f_{XX}$$

With Eq. (11), the computation of point $(N,K+1)$ proceeds as the computation of any other interior point. Similar considerations apply to the computation of point $(N-1,K+1)$.

If point $(N+1, K+1)$ is not available when applying Eq. (11), as is the case indicated in Fig. 3 where 2 shocks are

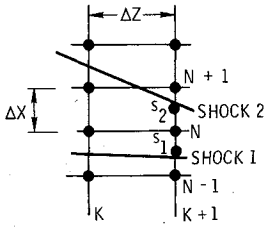

Fig. 3 Computation with closely spaced shocks.

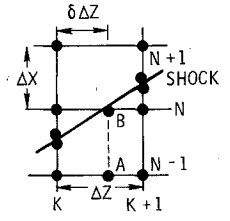

Fig. 4 Computation when a shock crosses a mesh line.

shown close to each other, then if the distance between the shocks is greater than ΔX, $\tilde{f}_X$ is approximated by

$$\tilde{f}_X = (\tilde{f}_{s2,K+1} - \tilde{f}_{s1,K+1}) / (\tilde{X}_{s2,K+1} - \tilde{X}_{s1,K+1}) \tag{12}$$

If, however, the distance between the shocks is smaller than ΔX, the values at $(N,K+1)$ are interpolated from the shock values.

When a discontinuity crosses a mesh line, the computation of this mesh point must be modified. In Fig. 4, an up-running shock is shown crossing the Nth mesh line between steps K and $K+1$. The usual interior point computation would require taking the one-sided difference between points $(N+K, K)$ and (N,K) for level one. This procedure is no longer proper, because of the presence of the shock. We, therefore, proceed by evaluating points A and B as follows

$$\left.\begin{aligned} f_A &= F_{N-1,K} + \delta(\tilde{f}_{N-1,K=1} - f_{N-1,K}) \\ f_B &= f_{s,K} + \delta(\tilde{f}_{s,K+1} - f_{s,K}) \end{aligned}\right\} \tag{13}$$

where

$$\delta = (X_N - X_{s,K}) / (\tilde{X}_{s,K+1} - X_{s,K}) \tag{14}$$

then, the value of f for level one at $(N, K+1)$ is

$$\tilde{f}_{N,K+1} = f_B + A_B (f_B - f_A)(1-\delta)\Delta Z/\Delta X \tag{15}$$

Care must be taken in evaluating δ when $dX_s/dZ \approx 0.$, since Eq. (14) becomes indeterminate. We therefore require that,

$$\left| \frac{dX_s}{dZ} \right| \Delta Z > 0.2\Delta X$$

otherwise, δ is set to one to give the desired result

$$\tilde{f}_{N,K+1} = \tilde{f}_{s,K+1}$$

A similar computation is performed when a down-running discontinuity crosses a mesh line.

V. Wall Computation

The compatibility equation, Eq. (4), is applied at the wall to evaluate P_Z

$$P_Z = -\partial P_X \pm \frac{\gamma w^2}{[\gamma T(\beta + w^2\tau^2)]^{1/2}} (\tau_Z + \lambda\tau_X) \tag{16}$$

where

$$\lambda = X_z + \lambda^{\pm} X_r$$

Here, the X derivatives are evaluated as three-point one-sided differences and

$$\tau_Z = \begin{cases} b_{zz} \text{ for } \lambda^- \\ c_{zz} \text{ for } \lambda^+ \end{cases}$$

Then, following the MacCormack algorithm, the value of the pressure at the wall, P_w, is given by

$$\tilde{P}_{w,K+1} = P_{w,K} + P_Z \Delta Z$$

$$P_{w,K+1} = \tfrac{1}{2}(P_{w,K} + \tilde{P}_{w,K+1} + \tilde{P}_Z \Delta Z)$$

With the pressure and entropy known at the wall, the temperature is obtained from Eq. (2), and the magnitude of the velocity from

$$\frac{u^2 + w^2}{2} + \frac{\gamma}{\gamma - 1} T = \text{constant} \tag{17}$$

The two-velocity component can then be determined from the known wall slope and the vanishing of the velocity component normal to the wall.

VI. Shock Detection

Perhaps the most distinguishing feature of the problem we are considering, and certainly its most troublesome one, is the possible formation of shock waves. In this section, we will consider the procedure required to detect an incipient shock. There are two important features for any such procedure. First, the procedure must be reliable. Incipient shocks must be located at the proper place, but most important, the procedure must be able to interpret the physics of the problem accurately, and should not be so sensitive as to create nonexistent shocks. Secondly, because the procedure must be executed at every step. it must be very fast and require a minimum amount of data to make a reliable decision.

The procedure we have constructed, based on the concept of coalescing characteristics, requires only information on 2 adjacent mesh points, and we find it to be both reliable and fast. However, its empirical nature should be kept in mind. It is applied at the end of a computational step as follows:

Assume that the flowfield is known at the Kth step (see Fig. 5). At each mesh point N and $N-1$, the up-running $(\lambda^+_N, \lambda^+_{N-1})$ and downrunning $(\lambda^-_N, \lambda^-_{N-1})$ characteristics are evaluated using Eq. (5). If we now assume that the ΔZ intervals between steps (evaluated from the CFL condition)[6] are essentially the same, then a quantity $\eta\pm$, which is the reciprocal of the number of steps needed for 2 characteristics to coalesce can be evaluated from

$$\eta\pm = (\lambda^{\pm}_{N-1} - \lambda^{\pm}_N)\Delta z/\Delta r$$

A considerable number of numerical experiments indicate that a shock should be fitted into the calculation when $\eta^{\pm}$ becomes greater than 0.22 (approximately 4 steps before the characteristics coalesce).

We have found that for a wide range of problems, if the detection of incipient shocks is delayed until $\eta^{\pm} < 0.22$), then the procedure becomes very sensitive and shocks are predicted unnecessarily.

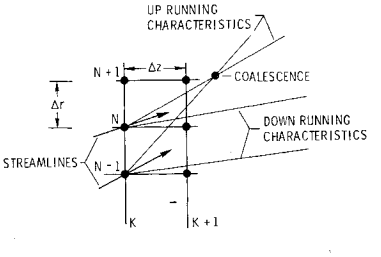

Fig. 5 Details of the shock detection.

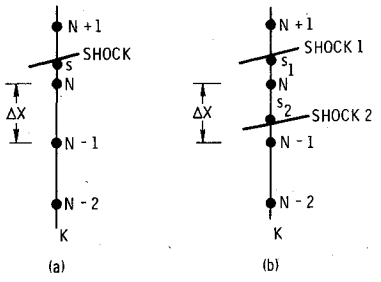

Fig. 6 Evaluation of the low-pressure side of a shock.

The detected shock is assumed to have the average slope of the coalescing characteristics and to be located half way between r_N and r_{N-1}. With the initial shock location known, the initial flowfield variables on the low pressure side are linearly interpolated between the 2 mesh points bracketing the shock, and on the high pressure side they are linearly extrapolated using the 2 mesh points next to the shock on the high pressure side.

Shocks that are generated at the walls of the duct, because of slope discontinuities at the walls, are introduced from user supplied information on the wall geometries, and do not make use of the procedure described in this section.

VII. Shock Computation

The low-pressure side of a shock is computed using the same scheme described for the interior point computation, but using the X derivatives given in this section. In Fig. 6, assuming that mesh point N lies on the low-pressure side, the X derivatives at the shock for the predictor level are evaluated from

$$f_{X_s}=\left[\frac{2}{1+\epsilon}\left(f_{s,K}-f_{N-1,K}\right)+0.5f_{N-2,K}-\frac{(0.5+\epsilon)}{(1+2\epsilon)}f_{N,K}\right]/\Delta X \tag{18}$$

where

$$\epsilon=(X_{s,K}-X_{N,K})/\Delta X \tag{19}$$

If only two mesh points are available, then the derivatives are evaluated from

$$f_{X_s}=\left[\frac{2\epsilon-1}{1+\epsilon}f_{N-1,K}+\frac{3}{1+\epsilon}f_{s,K}-2f_{N,K}\right]/\Delta X \tag{20}$$

with ϵ given by Eq. (19). The truncation error for Eq. (18) is of order ΔX^2 and for Eq. (20) it is

$$(\epsilon-1)\frac{\Delta X}{2}f_{XX_s}$$

It should be noted that Eqs. (18-20) are not the same formulas suggested by Moretti,[2,4] particularly Eq. (18) has a lower truncation error than Moretti's counterpart.

If only 1 mesh point is available (Fig. 6b), then f_{X_s} is approximated by

$$f_{X_s}=(f_{s1,K}-f_{s2,K})/(X_{s1,K}-X_{s2,K}) \tag{21}$$

provided that $(X_{s1,K}-X_{s2,K})$ is greater than ΔX. If $(X_{s1,K}-X_{s2,K})$ is smaller than ΔX, then f_{X_s} is set to zero. For the corrector stage, the same derivatives are used but with f replaced by $\bar{f}$.

If the low-pressure side lies on the other side of the shock, the derivatives that are used are the negatives of those given by Eq. (18) and Eq. (20), and ϵ is given by the negative of Eq. (19).

The computation of the high-pressure side of the shock has been formulated using the compatibility equation, Eq. (4), on the characteristic reaching the shock on the high-pressure side along with Rankine-Hugoniot conditions. The details of this classical treatment of the shock can be found in Ref. 4.

The computation of the high-pressure side was the only computation requiring involved programing logic. The main difficulty is the determination of the origin of the characteristic reaching the shock in the immediate vicinity of other discontinuities. It should be, however, possible to avoid these difficulties by computing the high-pressure side with the method suggested by Kentzer.[7]

VIII. Contact Surface Computation†

To compute a contact surface, we exploit the fact that both pressure and streamline slope are continuous across a contact surface. Eqs. (3a, b), which involve derivatives of P and τ only, are thus recast in terms of the computational coordinates (X,Z), and are integrated using the MacCormack scheme where the X derivatives are evaluated using Eq. (20). In the predictor level, Eq. (20) is applied on the high Mach number side of the contact surface. In the corrector level, it is applied on the low Mach number side. This choice is arbitrary, and the same results are obtained if the order is reversed.

With the pressure and entropy known at the contact surface, the magnitude of the velocity follows from Eq. (17), and the 2 velocity components can be determined from the evaluated streamline slope.

IX. Interactions

The interactions of the discontinuities with the walls of the duct and with each other are computed by locally exact solutions. The details of these calculations can be found in most text books in fluid mechanics, for example, Ref. 8, and will not be discussed here.

X. Elimination of Weak Discontinuity

Discontinuities with a Mach number difference across the discontinity of less than 1% are automatically eliminated from the computation. This feature is not a requirement of the technique. It has, however, been incorporated, because for most practical applications, tracing these weak discontinuties is not necessary. It speeds up the computation, and it avoids computing degenerate discontinuities (i.e. the contact surface formed by the interaction of 2 shock waves of equal strength).

XI. Results

The results of several calculations performed with the floating shock fitting technique are presented to demonstrate the accuracy and versatility of the technique. All the computations were done on a CDC 6600 computer. The core required to run the code is under 55000_8 locations.

The flowfield produced by a uniform flow impinging on a wedge is often used to validate numerical calculations. The problem is a trivial one, consisting of uniform properties in front and behind the shock wave. The exact solution for a freestream Mach number of 3.50 which is initially compressed by a 15° wedge and then expanded, such as to exactly cancel the shock wave generated by the wedge, is shown in Fig. 7. In the figure, the lower wall pressure distribution shown corresponds to the case where the expansion occurs a very short distance before the shock reflects from the wall. The exact solution is obtained with the floating shock fitting

†We have recently experienced some difficulties with this procedure when the contact surface is next to a strong expansion fan. The problems have been overcome by reformulating the contact surface computation along the guide lines discussed in the shock computation.

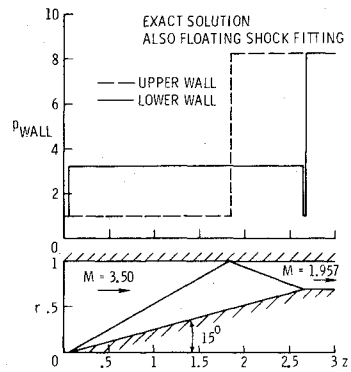

Fig. 7 Flowfield over a 15° wedge with shock cancellation.

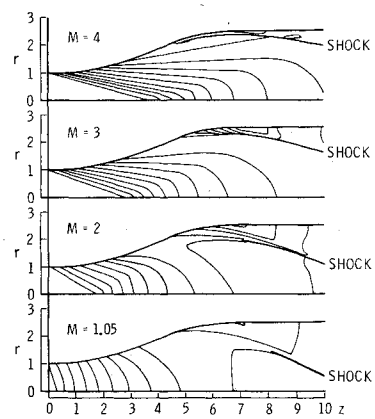

Fig. 8 Parametric study of a nozzle, showing shock waves and isobars.

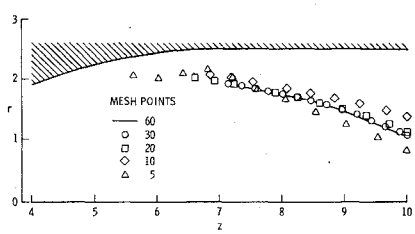

Fig. 9 Shock path for $M=1$ case.

technique using only 2 mesh points in less than 1 sec of computational time (the same results are obtained increasing the number of mesh points).

In Fig. 8, the results of a parametric study of the flowfield produced by a nozzle are presented. The initial Mach number was used as the parameter, allowing it to range from near 1 to 4. Both the isobars and shock-wave patterns are shown in the figure. For the Mach 4 case, most of the isobars downstream of the shock wave were not included in the figure to avoid overcrowding of lines. The total computational time for these 4 cases, using 30 mesh points, was approximately 25 sec. Figures 9 and 10 give some further details in the calculation of the Mach 2 case. In these 2 figures the results obtained with 5, 10, 20, 30, and 60 points are shown. Figure 9 shows the calculated shock-wave path, while Fig. 10 shows the upper wall pressure distribution. The results show that a good qualitative result for this more complicated problem can be obtained with as few as 5 mesh points, and that good quantitative results are obtained with only 10 mesh points.

It is very often argued that shock fitting is limited in its capability to handle flowfields with more than a single shock.[9-11] In Refs. 3 and 12 this has been shown not to be the case for very complex three-dimensional steady, and one-dimensional time-dependent flows. We hope to fill the existing gap for two-dimensional steady problems with Fig. 11 and also to demonstrate that floating shock fitting is a numerically stable technique even in multishocked flowfields. In Fig. 11, the geometry of NASA Langley's scramjet combustor model is simulated. The results shown are for a flow with an incoming Mach number equal to 3. inclined at 8° with the horizontal. The resulting flowfield con-

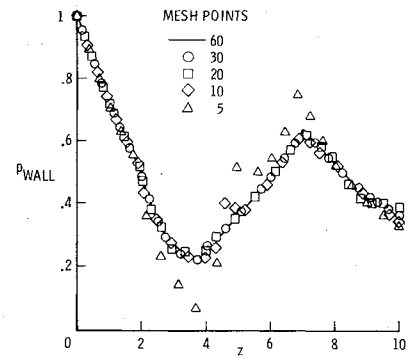

Fig. 10 Upper wall pressure for $M=2$ case.

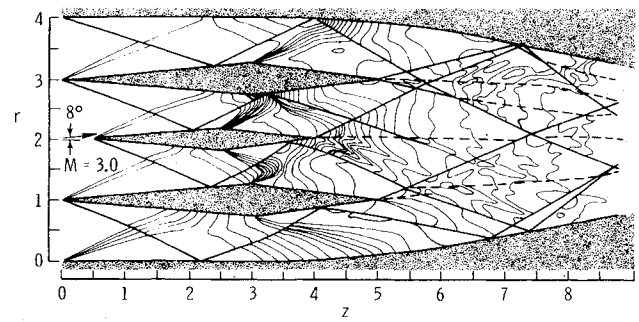

Fig. 11 Flowfield for a simulated scramjet, showing shock waves, vortex sheets and isobars.

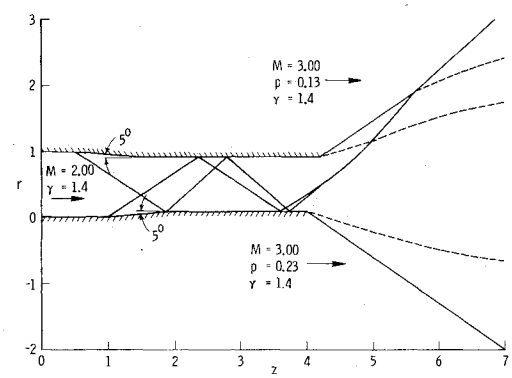

Fig. 12 Plume flowfield showing shock waves and vortex sheets.

sists of a complex pattern of interacting expansions and shock waves. In the figure, the shock-wave pattern is shown by the heavy lines. The contact surfaces are shown by the dashed lines, and isobars are shown by the light lines. Certain discontinuities are seen to terminate abruptly in the flowfield, while some shock interactions do not show the expected vortex sheet; this is a result of the automatic elimination of weak discontinuties previously discussed. The calculation was performed in 6 pieces, using a total of 120 mesh points and requiring approximately 2.2 min of computational time. The calculation shows approximately a dozen discontinuties, with some 40 interactions.

The technique has been extended to internal axisymmetric flows (with and without swirl), internal line source type flows, and to external two-dimensional flows. An example of the application to external flows is shown in Fig. 12, where a flow with an initial Mach number of 2.0 exhausts into a Mach 3.0 freestream. The lower wall ends at $z=4.0$, while the upper wall ends at $z=4.2$. The freestream conditions for the external flows are shown in the figure.

XII. Conclusions

Floating shock fitting for two-dimensional steady flows is an accurate and stable technique capable of solving very complex problems with acceptable running times. A fully three-dimensional code is planned for the near future.

References

[1]Moretti, G., "Three-Dimensional, Supersonic, Steady Flows With Any Number of Imbedded Shocks," AIAA Paper 74-10, Washington, D.C., 1974.

[2]Moretti, G., "Experiments in Multi-Dimensional Floating Shock Fitting," Polytechnic Institute of Brooklyn, PIBAL Rept. 73-18, Aug. 1973.

[3]Marconi,F. and Salas, M., "COMPUTATION OF Three-Dimensional Flows About Aircraft Configurations," *Computers and Fluids,* Vol. I, 1973, pp. 185-195.

[4]Moretti, G., "Thoughts and Afterthoughts About Shock Computations," Polytechnic Institute of Brooklyn, PIBAL Rept. 72-37, Dec. 1972.

[5]Richtmyer, R.D. and Morton, K.W., *Difference Methods for Initial-Value Problems,* Interscience Publishers, New York, 1967, p. 378.

[6]MacCormack, R.W., "The Effect of Viscosity in Hypervelocity Impact Cratering," AIAA Paper 69-354, Cincinnati, Ohio, 1969.

[7]Kentzer, C., "Discretization of Boundary Conditions on Moving Discontinuities," *Proceedings of the Second Int. Conf. on Numerical Methods in Fluid Dynamics,* Berkeley, Calif., Sept. 1970, pp. 108-113.

[8]Courant, R. and Friedrichs, K.O., *Supersonic Flow and Shock Waves,* Interscience Publishers, Inc., New York, Chapt. III.

[9]Vinokur, M., "Conservation Equations of Gasdynamics in Curvilinear Coordinate Systems," *Journal of Computational Physics,* Vol. 14, 1974, pp. 105-125.

[10]Kutler, P., Lomax, H., and Warming, R.F., "Computation of Space Shuttle Flow Fields Using Non-Centered Finite-Difference Schemes," AIAA Paper 72-193, San Diego, Calif., 1972.

[11]Kutler, P., and Reinhardt, W.A., "Numerical Computation of Multi-Shocked Three-Dimensional Supersonic Flow Fields With Real Gas Effects," AIAA Paper 72-702, Boston, Mass., 1972.

[12]Moretti, G., "Complicated One-Dimensional Flows," Polytechnic Institute of Brooklyn, PIBAL 71-25, Sept. 1971.